Published in final edited form as:
Nat Mater. 2009 September ; 8(9): 747–751. doi:10.1038/nmat2509.

A dual-emissive-materials design concept enables tumour hypoxia imaging

Guoqing Zhang[1], **Gregory M. Palmer**[2], **Mark W. Dewhirst**[2], and **Cassandra L. Fraser**[1,*]

[1]Department of Chemistry, University of Virginia, Charlottesville, Virginia 22904, USA

[2]Department of Radiation Oncology, Duke University Medical Center, Durham, North Carolina 27710, USA

Abstract

Luminescent materials are widely used for imaging and sensing owing to their high sensitivity, rapid response and facile detection by many optical technologies1. Typically materials must be chemically tailored to achieve intense, photostable fluorescence, oxygen-sensitive phosphorescence or dual emission for ratiometric sensing, often by blending two dyes in a matrix. Dual-emissive materials combining all of these features in one easily tunable molecular platform are desirable, but when fluorescence and phosphorescence originate from the same dye, it can be challenging to vary relative fluorescence/phosphorescence intensities for practical sensing applications. Heavy-atom substitution[2] alone increases phosphorescence by a given, not variable amount. Here, we report a strategy for modulating fluorescence/phosphorescence for a single-component, dual-emissive, iodide-substituted difluoroboron dibenzoylmethane-poly(lactic acid) (BF_2dbm(I)PLA) solid-state sensor material. This is accomplished through systematic variation of the PLA chain length in controlled solvent-free lactide polymerization[3] combined with heavy-atom substitution2. We demonstrate the versatility of this approach by showing that films made from low-molecular-weight BF_2dbm(I)PLA with weak fluorescence and strong phosphorescence are promising as 'turn on' sensors for aerodynamics applications[4], and that nanoparticles fabricated from a higher-molecular-weight polymer with balanced fluorescence and phosphorescence intensities serve as ratiometric tumour hypoxia imaging agents.

Ratiometric sensing addresses challenges associated with sensor concentration and obviates the need for specialized luminescence lifetime instrumentation. For example, Kopelman and co-workers developed a powerful nanosensor (PEEBLEs) for ratiometric oxygen sensing comprising a cyanine dye standard and an O_2-sensitive Pt porphyrin phosphor in a sol–gel matrix and demonstrated its utility for cell biology[5]. Single-component dye-polymer conjugates with both fluorescence and phosphorescence offer advantages over three-component dye/standard/matrix mixtures. Dual-emissive materials possess an internal rather than external standard in ratiometric sensing schemes, and thus, 1:1 fluorophore/phosphor stoichiometry, resulting in greater sample homogeneity and minimal dye leaching. Readily processable biomaterials combined with photostable, optically tunable dyes that emit brightly even in aqueous environments are beneficial for imaging and sensing in biomedical contexts.

*fraser@virginia.edu.

Author contributions

G.Z and C.L.F. are responsible for materials design, synthesis and characterization and manuscript preparation. G.M.P. and M.W.D. are responsible for tumour hypoxia imaging studies and data analysis.

Previously, we discovered that difluoroboron dibenzoylmethane-poly(lactic acid) (BF_2dbmPLA; as in Fig. 1, with hydrogen in place of iodide) exhibits unusual, long-lived green room-temperature phosphorescence (RTP) in addition to intense blue fluorescence[6]. Given that thermal decay pathways are often accessible, it is rare to see RTP from organic compounds; typically organized media7,8 or heavy atoms9 are required for RTP. This feature adds enhanced capability to the excellent fluorescence properties of boron dyes[10,11] and materials[12,13]. Nanoparticles fabricated from BF_2dbmPLA and related analogues show great promise for *in vitro* and *in vivo* imaging and oxygen sensing[14]. Although BF_2dbmPLA singlet and triplet emission are clearly distinguished on the basis of wavelength (λ_F = 440 nm, λ_P = 509 nm) and lifetime (τ_F = 2 ns, τ_P = 170 ms), the high singlet quantum yield ($\Phi_F \sim 0.80$) and much weaker RTP preclude the use of this first-generation material as a practical intensity-based ratiometric sensor. Ideally, much stronger phosphorescence intensity is required for ratiometric sensing. For insight into how to achieve this goal and modulate relative fluorescence to phosphorescence intensities, we turn to quantum theory.

According to perturbation theory, for a polyatomic molecule, the perturbation factor δ describing singlet–triplet mixing by first-order spin–orbit coupling can be expressed as in equation (1) (ref. 2),

$$\delta = \frac{\left\langle {}^3\Psi | H_{so} | {}^1\Psi \right\rangle}{|E_1 - E_3|} \quad (1)$$

where ${}^1\Psi$ and ${}^3\Psi$ are the wavefunctions of singlet and triplet states, respectively, H_{so} is the spin–orbit Hamiltonian and E_1 and E_3 are the energy levels for singlet and triplet states. This expression indicates that a greater spin–orbit matrix value and a smaller energy gap $|E_1 - E_3|$ correspond to a larger δ; that is, a high probability of electronic transition between singlet and triplet states. The spin–orbit matrix elements are highly sensitive to the atomic number of the atoms in the vicinity of the exciton. Heavy atoms either in the environment (external), or part of the luminescent molecule (internal) can enhance spin–orbit coupling and thus, increase the rate of intersystem crossing. Since the discovery of the internal heavy-atom effect by McClure15 in 1949, halogens or large-atomic-number metals have been incorporated into luminescent molecules to enhance RTP intensity relative to fluorescence2. For example, heavy-atom-based RTP materials can improve the light-emitting diode device16 efficiency in that triplet excitons may be the main (75%) excited-state species on electron–hole recombination17. The singlet–triplet energy gap, $|E_1 - E_3|$, on the other hand, may be controlled by boron dye loading, or in the case of dye-polymer conjugates, polymer-chain molecular weight. We have shown that fluorescence emission for BF_2dbmPLA powders varies over a 64 nm range depending on BF_2dbmPLA molecular weight (3–20 kDa, 507–443 nm respectively)[3]. High-molecular-weight samples exhibit blueshifted emission similar to solution, whereas increased fluorophore–fluorophore interactions in low-molecular-weight materials correspond to lower-energy, redshifted fluorescence.

Phosphorescence, in contrast, showed little change in energy or relative intensity with BF_2dbmPLA molecular weight, suggesting that heavy-atom substitution may be necessary to augment the molecular-weight effect. On the basis of these arguments and previous observations, phosphorescence intensity is expected to be strongest for internal heavy-atom-modified materials with low molecular weights.

To test this idea, BF_2dbm(I)PLA samples with different molecular weights (**P1** = 2,700 Da, **P2** = 7,300 Da and **P3** = 17,600 Da) were prepared from a BF_2dbm(I)OH initiator, **1**, and lactide by solvent-free, tin-catalysed, controlled ring-opening polymerization (Fig. 1a, Supplementary Table S1). Polymers with low polydispersity indices (PDIs < 1.2) were obtained. The optical

properties of **P1**–**P3** were first investigated in CH_2Cl_2 under air (Table 1). Under these conditions, all three polymers have nearly identical absorption (λ_{abs} = 406 nm) and emission spectra ($\lambda_F \sim 435$ nm, $\Phi_F \sim 0.4$, $\tau_F \sim 0.95$ ns) (see Supplementary Figs S1 and S2). As expected, iodide substitution results in enhanced intersystem crossing, lower Φ_F and shorter τ_F compared with hydrogen-substituted BF_2dbmPLA (ref. 6). Phosphorescence is absent for **P1**–**P3** in solution; RTP is a solid-state effect for these boron biomaterials.

For BF_2dbm(I)PLA powders, RTP and molecular-weight-dependent fluorescence emission colour tuning are expected and indeed observed. Correspondingly, two distinct emission bands were observed in spectra for **P2** (470 nm, 527 nm) and **P3** (456 nm, 525 nm), whereas, for low-molecular-weight **P1**, a single emission peak at 535 nm was evident with only a small shoulder at ~480 nm (Fig. 1c, Table 2). The higher energy band is attributed to fluorescence and the other much stronger, redshifted band is RTP emission. Under nitrogen, the emission colours of **P1**–**P3** are greenish yellow, green and cyan respectively (Fig. 1g). Just as equation (1) predicts, as the energy gap, ΔE, decreases (that is, BF_2dbm(I)PLA molecular weight decreases), the singlet–triplet coupling becomes stronger (that is, larger δ), intersystem crossing is favoured and RTP intensity increases.

Luminescence lifetime data were also collected for **P1**–**P3** as powders (Table 2). All lifetimes fit to triple-exponential decay owing to the heterogeneity of the polymer matrix and possibly fluorophore–fluorophore interactions too. The fluorescence lifetimes become shorter (0.43–0.37 ns) as the polymer chain decreases (17.6–2.7 kDa) presumably owing to enhanced intersystem crossing (Table 1). Shorter RTP and delayed fluorescence lifetimes (**P1**–**P3:** 4.50–4.06 ms) with decreasing molecular weight suggest smaller singlet–triplet energy splitting where the thermal repopulation from triplet to singlet states is more probable[3]. Surprisingly, when the samples were exposed to air, long-lived RTP was still detectable (0.42, 0.55, 0.57 ms for **P1**–**P3**, respectively; see Supplementary Table S2). Consistent with the spectral data in Fig. 1b where RTP bands remain visible, these results indicate a much faster triplet decay rate compared with BF_2dbmPLA, which is entirely quenched in air. This suggests that radiative decay occurs on a comparable timescale to dynamic quenching, which is probably influenced by O_2 diffusion rates in the material[18].

Although the model predicts the observed fluorescence/phosphorescence control through heavy-atom assistance and polymer molecular weight, the experimental results exceeded our expectations. We discovered a tunability range that is nearly ideal, in terms of control and flexibility in oxygen sensor design. All **P1**–**P3** materials, regardless of molecular weight can be useful in lifetime or time-gated intensity-based sensing platforms. Those with comparable and readily detectable fluorescence and phosphorescence intensities (for example, **P2**) are beneficial for ratiometric hypoxia imaging, whereas, low-molecular-weight materials with weak to negligible fluorescence and strong phosphorescence (**P1**) serve as ‘turn on’ sensors that light up in anaerobic or low-oxygen environments. A simple demonstration of these effects is presented in Fig. 1, which shows changes in colour and brightness for **P1**–**P3** films under air (Fig. 1f) versus nitrogen (Fig. 1g). Thus, with a very simple molecular-weight adjustment, these boron biomaterials are easily tailored for different sensor platforms and imaging and detection schemes.

To explore oxygen sensitivity and processing effects in more detail and to demonstrate the relevance and versatility of this materials design concept for practical applications, boron biomaterials were fabricated as thin films and nanoparticles. Polymers **P1**–**P3** were cast from CH_2Cl_2 solutions (5 mg ml^{-1}, or 0.3% w/w) onto glass substrates, followed by annealing at ~110 ° C for 10 s to improve film clarity. Under nitrogen, all three films showed visibly blueshifted colours compared with the powders. The steady-state emission spectra under air and nitrogen are given in Fig. 1d and e respectively, where it is noted that the fluorescence

contributions are clearly larger than for the bulk polymer samples. Film fluorescence lifetimes are longer than their powder counterparts, suggesting decreased intersystem crossing perhaps due to diminished fluorophore–fluorophore interactions.

As a starting point for ratiometric oxygen sensing, the steady-state emission spectra of the **P1** film were recorded under different O_2 concentrations (Fig. 2a). The ratio of the invariant fluorescence (λ_F = 458 nm) to the oxygen-dependent RTP (λ_P = 532 nm) steadily increases with increasing oxygen levels (Fig. 2c). Up to 1% O_2, a linear dependency is observed (R^2 = 0.996). Beyond this point, the fluorescence/phosphorescence plot continues to rise up to ambient levels (that is, 21% O_2) but with curvature (Supplementary Fig. S3), possibly due to complicated dynamics in the heterogeneous polymer environment as previously reported[6]. Figure 2b shows the oxygen distribution on the surface of a **P1** film under ultraviolet excitation (λ_{ex} = 365 nm), where the bright yellow streaks provide clear visualization of nitrogen gas flow dynamics.

The polymer **P2**, with balanced fluorescence and phosphorescence emission, was also fabricated as boron nanoparticles (BNPs; 98 nm diameter) by nanoprecipitation[14]. The emission spectra (λ_F = 450 nm, λ_{RTP} = 528 nm; Supplementary Fig. S4), lifetimes (τ_F ~ 0.45 ns, τ_{RTP} ~ 4.82 ms) and oxygen calibration (Supplementary Fig. S5) are comparable to **P2** films. Fortuitously, the optimal linear range for this nanosensor (~0–3%) is in excellent correspondence with hypoxia in biological contexts. For example, tumour hypoxia (pO_2 < 1%; ref. 19) is associated with increased invasiveness and resistance to radiation and chemotherapy. Despite its importance for cancer treatment and tumour biology[20], hypoxia is difficult to image with good spatial and temporal resolution, particularly in combination[21]. Given their small size, biocompatibility, photostability, dual-emissive features and high oxygen sensitivity, BNPs have the potential to address some of these challenges. To test their ability as ratiometric tumour hypoxia imaging agents, **P2** nanoparticles were used in combination with a mouse dorsal window chamber breast cancer 4T1 mammary carcinoma model for hyperspectral imaging[22]. Tissue oxygen maps of the window region presented as fluorescence/phosphorescence ratios during carbogen, air and brief nitrogen breathing (95, 21 and 0% O_2 respectively), show excellent contrast between the microvasculature (red) and the tumour tissue (blue), which remained hypoxic regardless of the breathing gas (Fig. 3). The signal was relatively stable ~1–2 min after changing the breathing gas, which may be a function of the biology of tissue oxygen delivery and consumption more so than the inherent response of the nanosensors. The BNP tumour oxygenation maps are complementary to existing optical methods such as haemoglobin saturation imaging, which provides vascular oxygenation[22].

We have devised a simple yet powerful strategy for systematically tuning relative fluorescence and RTP intensities in a dual-emissive boron biomaterial. The experimental results support the proposed design concept involving manipulation of both spin–orbit coupling and singlet–triplet energy splitting. The wide-range fluorescence/phosphorescence tunability of boron biomaterials enables application in lifetime, time-gated intensity, ratiometric or ‘turn on’ sensing modes, and shows great promise for optical imaging, oxygen sensing and aerodynamics applications[4]. A new method for quantifying tumour hypoxia has also been demonstrated, and can further understanding of the relationship between hypoxia, tumour progression, metastasis and treatment resistance. This first demonstration of hypoxia imaging bodes well for using boron biomaterials for oxygen sensing in other biomedical and biotechnological contexts.

Methods

Molecular weights were determined by gel permeation chromatography (tetrahydrofuran, 20 °C, 1.0 ml min^{-1}) versus polystyrene standards on a Hewlett-Packard instrument (series 1100 HPLC) equipped with Polymer Laboratories 5 μm mixed-C columns and connected to

ultraviolet–visible and refractive index (Viscotek LR 40) detectors. A 0.58 correction factor was applied[23,24]. Data were processed with the OmniSEC software (version 4.2, Viscotek Corp). Ultraviolet–visible spectra were recorded on a Hewlett-Packard 8453 diode array spectrophotometer. Photographs were taken in the dark using a Canon PowerShot SD600 Digital Elph camera with the automatic setting (no flash).

Powders were analysed as precipitated. A Laurell Technologies WS-650S spin-coater was used to cast polymer films for luminescence measurements with the default set-up (30 s at a constant speed of 4,000 r.p.m.). Boron polymer films were spin-cast from CH_2Cl_2 solutions (~2.5% w/w) onto Fischer Scientific glass cover slides (22 × 22 mm) at a spin speed of 4,000 r.p.m. The coated slides were cut into ~3 mm × 22 mm strips, placed in a transparent glass vial under a N_2 atmosphere and were sealed with Teflon caps for measurements. (Note: both borosilicate glass cover slides and glass vials are optically inactive using an excitation wavelength of greater than 368 nm.)

Steady-state fluorescence emission spectra were recorded on a Horiba Fluorolog-3 Model FL3-22 spectrofluorometer (double-grating excitation and double-grating emission monochromators). For all luminescence measurements, a Tiffen 55 mm 0.9 neutral density filter was placed in the path of the excitation source to protect the sample from photobleaching. RTP spectra were recorded with the same instrument except that a pulsed xenon lamp (λ_{ex} = 369 nm; duration < 1 ms) was used and spectra were collected with a 1 ms delay after excitation. Time-correlated single-photon counting fluorescence lifetime measurements were carried out with a NanoLED-370 (369 nm) excitation source and a DataStation Hub as the single-photon counting controller. Phosphorescence lifetimes were measured with a 500 ns multi channel scalar card excited with a pulsed xenon lamp (λ_{ex} = 369 nm; duration < 1 ms). Lifetime data were analysed with DataStation v2.4 software from Horiba Jobin Yvon.

Fluorescence quantum yields, Φ_F, for BF_2dbm(I)OH (**1**) and BF_2dbm(I)PLA (**P1**–**P3**) in CH_2Cl_2 were calculated versus anthracene in ethanol as a standard, as previously described[25] using the following values: Φ_F anthracene = 0.27 (ref. 26), n_D^{20} ethanol=1.360, n_D^{20} CH_2Cl_2=1.424; n_D^{20} is the refractive index (20 °C, yellow sodium D line, 589 nm). Optically dilute CH_2Cl_2 solutions of BF_2dbm(I)OH and BF_2dbm(I)PLA, and ethanol solutions of the anthracene standard were prepared in 1-cm-path-length quartz cuvettes, and absorbances (A < 0.1) were recorded and steady-state emission spectra were obtained (λ_{ex} = 350 nm; emission integration range: 365–700 nm).

For oxygen sensitivity and intensity-based Stern–Volmer plot measurements, gas mixtures of O_2 and N_2 of various concentrations were prepared by using two Cole-Parmer 65mm flow meters. For each concentration, the pre-mixed gas was passed through a 1-m-path quartz fluorometer cell equipped with a septum screw top containing the spin-cast **P1** film for 15 min and then the spectrum was recorded. The oxygen sensitivity for the **P2** nanoparticle aqueous suspension was calibrated similarly except that the pre-mixed gas was first evenly dispensed into a distilled-water chamber before passing through a quartz cell containing 1 ml of the optically dilute (abs < 0.1) sample.

A window chamber was implanted using previously described techniques[22]. Briefly, the mouse was anaesthetized using an intraperitoneal injection of 100 mg kg^{-1} ketamine, 10 mg kg^{-1} xylazine. The skin on the back of the animal was stretched into a metal frame to enable insertion of a titanium window frame, having a 12-mm-diameter window. The front face of the skin fold was excised, and approximately 20,000 4T1 murine mammary carcinoma cells were injected into the underlying fascia. A cover glass was placed over the open face of the window, and the tumour was allowed to incubate for 10 days before imaging.

An approximately 100 μl suspension of **P2** nanoparticles (~1 mg ml^{-1}) was injected into the space between the window chamber and the cover glass. Approximately 5 min passed between the injection and imaging, which allowed for stabilization of the signal. The animal was placed on an upright fluorescence microscope equipped with a DAPI excitation filter, and a liquid-crystal tunable emission filter (VariSpec, Cambridge Research and Instrumentation). This enabled acquisition of an emission spectrum, which was acquired in 10 nm intervals from 430 to 600 nm. Gas was administered by a nose cone at a rate of 5 l min^{-1}, except for room air, during which the gas was shut off. The carbogen breathing was begun at the beginning of the experiment, with approximately 5 min passing before the initial acquisition. The gas was then switched to room air for a period of 3 min, and finally nitrogen for 30 s. The images shown in Fig. 3 were taken at the end of each respective period of gas breathing. Data were processed by taking the ratio of the fluorescence to phosphorescence signals, which were defined as the average signal acquired from 430 to 480 nm and 530 to 600 nm, respectively.

Supplementary Material

Refer to Web version on PubMed Central for supplementary material.

Acknowledgments

We thank the National Science Foundation (C.L.F.: CHE 0718879), the Department of Defense (G.M.P.: Postdoctoral Fellowship W81XWH-07-1-0355) and the NIH (M.W.D.: R01CA40355) for support for this research. We are also grateful to the UVA NanoSTAR Institute and the UVA Cancer Center through the James and Rebecca Craig Foundation and the NCI Cancer Center Support Grant P30 CA44579 for supporting our efforts to develop and test BNPs as biomedical imaging agents. We thank J. N. Demas for helpful discussions and R. E. Evans for assistance.

References

1. Yuste R. Fluorescence microscopy today. Nature Methods 2005;2:902–904. [PubMed: 16299474]
2. Lower SK, El-Sayed MA. The triplet state and molecular electronic processes in organic molecules. Chem. Rev 1966;66:199–241.
3. Zhang G, Kooi SE, Demas JN, Fraser CL. Emission colour tuning with polymer molecular weight for boron dibenzoylmethane-polylactide. Adv. Mater 2008;20:2099–2104.
4. Köse ME, Omar A, Virgin CA, Carroll BF, Schanze KS. Principal component analysis calibration method for dual-luminophore oxygen and temperature sensor films: Application to luminescence imaging. Langmuir 2005;21:9110–9120. [PubMed: 16171340]
5. Koo YEL, et al. Real-time measurements of dissolved oxygen inside live cells by organically modified silicate fluorescent nanosensors. Anal. Chem 2004;76:2498–2505. [PubMed: 15117189]
6. Zhang G, et al. Multi-emissive difluoroboron dibenzoylmethane polylactide exhibiting intense fluorescence and oxygen sensitive room temperature phosphorescence. J. Am. Chem. Soc 2007;129:8942–8943. [PubMed: 17608480]
7. Scypinski S, Love LJC. Room-temperature phosphorescence of polynuclear aromatic hydrocarbons in cyclodextrins. Anal. Chem 1984;56:322–327.
8. Mitchell CA, Gurney RW, Jang S-H, Kahr B. On the mechanism of matrix-assisted room temperature phosphorescence. J. Am. Chem. Soc 1998;120:9726–9727.
9. Carretero AS, Castillo AS, Gutiérrez AF. A review of heavy-atom-induced room-temperature phosphorescence: A straightforward phosphorimetric method. Crit. Rev. Anal. Chem 2005;35:3–14.
10. Chow YL, Cheng XC, Johansson CI. Molecular interactions of dibenzoylmethanatoboron difluoride ($DBMBF_2$) in the excited and ground states in solution. J. Photochem. Photobiol. A 1991;57:247–255.
11. Cogné-Laage E, et al. Diaroyl(methanato)boron difluoride compounds as medium sensitive two-photon fluorescent probes. Chem. Eur. J 2004;10:1445–1455.
12. Nagai A, Kokado K, Nagata Y, Chujo Y. 1,3-Diketone-based organoboron polymers: Emission by extending π-conjugation along a polymeric ligand. Macromolecules 2008;41:8295–8298.

13. Qin Y, Kiburu I, Shah S, Jäkle F. Synthesis and characterization of organoboron quinolate polymers with tunable luminescence properties. Macromolecules 2006;39:9041–9048.

14. Pfister A, Zhang G, Zareno J, Horwitz AF, Fraser CL. Boron polylactide nanoparticles exhibiting fluorescence and phosphorescence in aqueous medium. ACS Nano 2008;2:1252–1258. [PubMed: 19081748]

15. McClure DS. Triplet–singlet transitions in organic molecules. Lifetime measurements of the triplet state. J. Chem. Phys 1949;17:905–913.

16. Adachi C, Baldo MA, Thompson ME, Forrest SR. Nearly 100% internal phosphorescence efficiency in an organic light-emitting device. J. Appl. Phys 2001;90:5048–5051.

17. Baldo MA, O'Brien DF, Thompson ME, Forrest SR. Excitonic singlet–triplet ratio in a semiconducting organic thin film. Phys. Rev. B 1999;60:14422–14428.

18. Twarowski AJ, Good L. Phosphorescence quenching by molecular oxygen: Zinc tetraphenylporphin on solid supports. J. Phys. Chem 1987;91:5252–5257.

19. Höckel M, Vaupel P. Tumor hypoxia: Definitions and current clinical, biologic, and molecular aspects. J. Natl Cancer Inst 2001;93:266–276. [PubMed: 11181773]

20. Harris AL. Hypoxia—a key regulatory factor in tumour growth. Nature Rev. Cancer 2002;2:38–47. [PubMed: 11902584]

21. Dewhirst MW, et al. Review of methods used to study oxygen transport at the microcirculatory level. Int. J. Cancer 2000;90:237–255. [PubMed: 11091348]

22. Sorg BS, Moeller BJ, Donovan O, Cao Y, Dewhirst MW. Hyperspectral imaging of hemoglobin saturation in tumor microvasculature and tumor hypoxia development. J. Biomed. Opt 2005;10:44004. [PubMed: 16178638]

23. Baran J, Duda A, Kowalski A, Szymanski R, Penczek S. Intermolecular chain transfer to polymer with chain scission: General treatment and determination of k_p/k_{tr} in L, L-lactide polymerization. Macromol. Rapid Commun 1997;18:325–333.

24. Save M, Schappacher M, Soum A. Controlled ring-opening polymerization of lactones and lactides initiated by lanthanum isopropoxide, 1. General aspects and kinetics. Macromol. Chem. Phys 2002;203:889–899.

25. Crosby GA, Demas JN. Measurement of photoluminescence quantum yields. J. Phys. Chem 1971;75:991–1024.

26. Melhuish WH. Quantum efficiencies of fluorescence of organic substances: Effect of solvent and concentration of the fluorescent solute. J. Phys. Chem 1961;65:229–235.

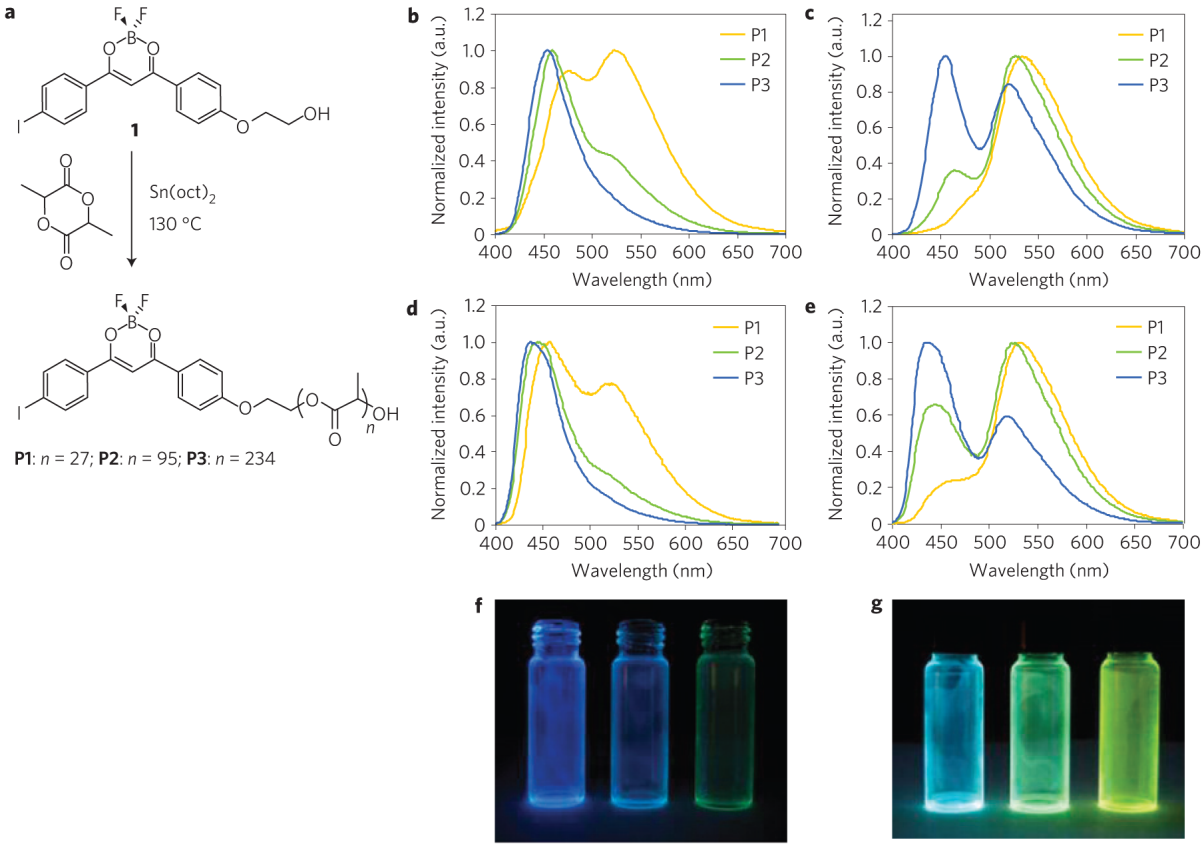

Figure 1. Synthesis and solid-state emission of BF_2dbm(I)PLA (P1-P3)

a, Ring-opening polymerization of BF_2dbm(I)PLA (**P1-P3**). **b-e**, Steady-state emission spectra of polymers **P1-P3** as powders (**b,c**) and spin-cast films (**d,e**) under air (**b,d**) and under N_2 (**c,e**). **f,g**, Simple-cast **P1-P3** (right to left) films in vials under air (**f**) and N_2 (**g**) (ultraviolet excitation: λ_{ex} = 365 nm).

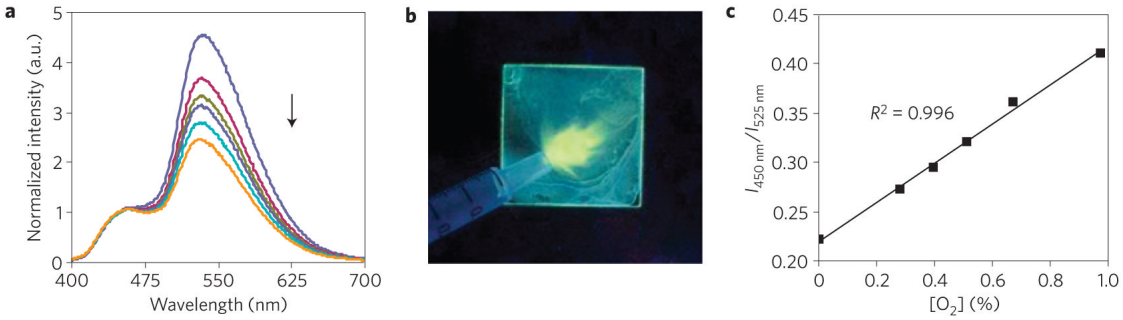

Figure 2. Oxygen sensitivity for P1 BF_2dbm(I)PLA film

a, Emission spectra of the spin-cast film (**P1**) under increasing oxygen levels (indicated by the arrow, 0-1%) normalized to the fluorescence band. **b**, Image showing yellow phosphorescence emission under a N_2 gas stream for a spin-cast **P1** film under ultraviolet excitation. (Yellow phosphorescence turns on immediately on gas contact. Blue green background: weak **P1** fluorescence.) **c**, Linear relationship between oxygen level and the fluorescence/ phosphorescence intensity ratio at two fixed wavelengths (450 nm and 525 nm).

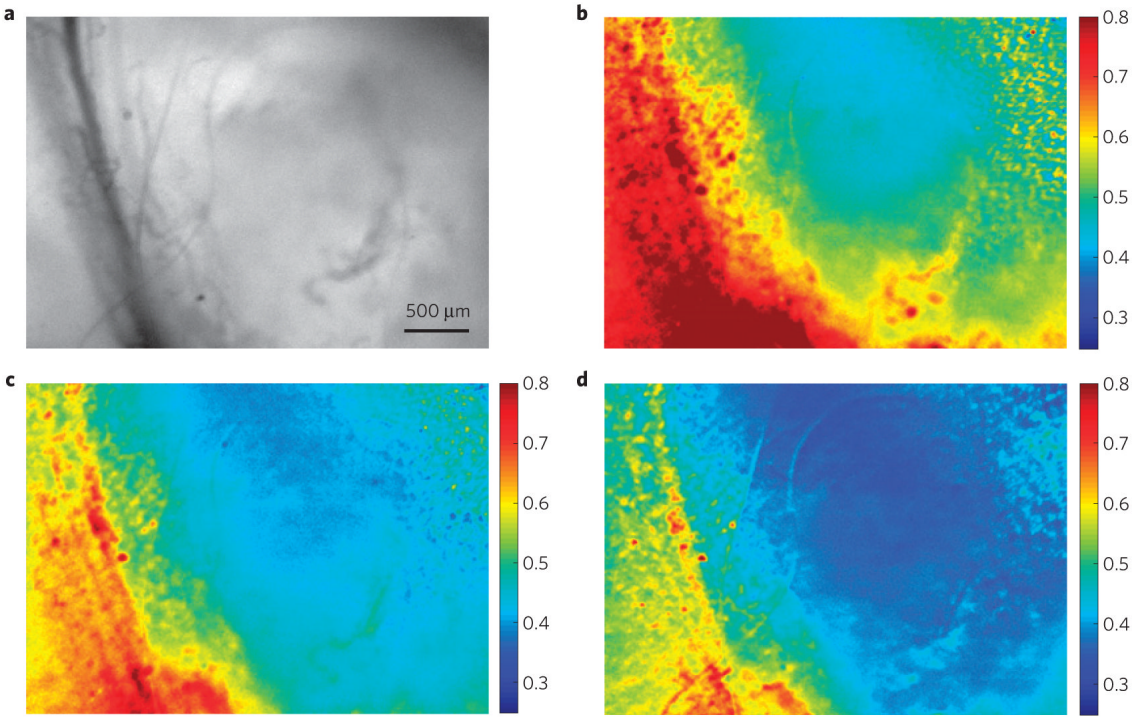

Figure 3. Tumour hypoxia imaging with P2 BF_2dbm(I)PLA nanoparticles

a-c, *In vivo* imaging of the breast cancer 4 T1 mammary carcinoma tumour region in a mouse window chamber model showing the bright-field (**a**) and BNP fluorescence/phosphorescence ratio while breathing carbogen—95% O_2 (**b**), room air—21% O_2 (**c**) and nitrogen—0% O_2 (**d**). Emission intensity was averaged from 430 to 480 nm (fluorescence) and 530 to 600 nm (phosphorescence). Several blood vessels run vertically on the left side of the images (dark lines in the bright-field image; more oxygenated yellow-red regions in the fluorescence/phosphorescence images), with the tumour comprising the region to the right of the vessels (less-oxygenated blue regions in the fluorescence/phosphorescence images).

Table 1

Characterization of polymers P1-P3 in solution

	M_n (Da)*	PDI†	λ_{abs} (nm)‡	ε (M^{-1} cm^{-1})‡	λ_F (nm)§	Φ_F¶	τ_F (ns)//
1	458	1	407	58,000	441	0.55	1.03
P1	2,700	1.11	406	33,000	435	0.41	0.95
P2	7,300	1.15	406	40,000	436	0.44	0.96
P3	17,600	1.17	406	40,700	435	0.43	0.95

*In tetrahydrofuran versus polystyrene standards.

†Polydispersity index (PDI)=M_w/M_n.

‡ε: molar extinction coefficient. In CH_2Cl_2.

§Steady-state fluorescence spectra excited at 369 nm.

¶Fluorescence quantum yields in CH_2Cl_2 relative to anthracene in ethanol.

//In CH_2Cl_2; excitation source: 369nm light-emitting diode; fluorescence lifetime fit to single-exponential decay.

Table 2

Luminescence characterization of P1-P3 in the solid state at 24 °C under nitrogen

	Powder				Film			
	λ_F* (nm)	τ_F† (ns)	λ_{RTP}‡ (nm)	τ_{RTP}§ (ms)	λ_F* (nm)	τ_F† (ns)	λ_{RTP}‡ (nm)	τ_{RTP}§ (ms)
P1	485	0.37	535	4.06	458	0.48	532	4.25
P2	470	0.42	527	4.39	445	0.54	526	4.37
P3	456	0.43	525	4.50	438	0.64	523	4.41

*Steady-state fluorescence spectra excited at 369 nm.

†Excitation source: 369nm light-emitting diode; fluorescence lifetime fit to triple-exponential decay.

‡Excitation source: xenon flash lamp at 405 nm.

§Excitation source: xenon flash lamp at 405 nm; RTP lifetime fit to triple-exponential decay.